

## ARTICLE

Two-way acoustic wave-equation-based  
wavefield depth extrapolation for imaging in  
vertically transversely isotropic mediaShanzheng Hu<sup>1,2</sup>, Pengyuan Sun<sup>1,2</sup>, Shuqin Li<sup>1,2</sup>, Feng Hu<sup>1,2</sup>, Min Guan<sup>1,2</sup>, and  
Jiachun You<sup>3\*</sup> <sup>1</sup>BGP Inc., China National Petroleum Corporation, Zhuozhou, Hebei, China<sup>2</sup>National Engineering Research Center of Oil and Gas Exploration Computer Software, China National Petroleum Corporation, Zhuozhou, Hebei, China<sup>3</sup>Department of Geophysics, Chengdu University of Technology, Chengdu, Sichuan, China(This article belongs to the *Special Issue: Advanced Artificial Intelligence Theories and Methods for Seismic Exploration*)

## Abstract

Anisotropy is a prevalent characteristic of the Earth's subsurface, giving rise to more complex wavefield behavior than in purely acoustic media. Seismic data acquired in such anisotropic environments pose significant challenges for conventional acoustic imaging methods that rely on isotropic assumptions and acoustic approximations, often leading to inaccurate imaging of complex geologic structures. To address these challenges, we propose a wavefield depth extrapolation method grounded in the two-way acoustic anisotropic wave equation, specifically tailored for imaging in vertically transversely isotropic (VTI) media. Theoretically, the proposed method extends the two-way wave-equation-based wavefield extrapolation framework from acoustic media to anisotropic VTI media. To further improve image quality, we used a frequency–wavenumber-domain approach to remove pseudo-S-wave energy, enhancing the clarity of P-wave descriptions and reducing imaging artifacts. We evaluated the effectiveness of the proposed approach through several numerical tests, including experiments on a VTI three-layer model, the Hess VTI model, and the Marmousi VTI model. These benchmarks demonstrated that our method consistently outperformed conventional acoustic schemes designed for isotropic media, yielding clearer, higher-resolution structural images. In addition, we applied both the acoustic and the VTI-based migration methods to a real seismic dataset. The VTI-based migration provided a clearer, more continuous image of the deep structures than the acoustic migration method. The numerical experiments and real data application demonstrated that the proposed VTI imaging strategy is both practical and effective. More importantly, the findings underscore the need to explicitly account for anisotropic parameters in seismic imaging workflows to achieve geologically consistent and reliable interpretations in VTI-dominated regions.

**Keywords:** Vertically transversely isotropic media; Two-way acoustic wave equation; Wavefield depth extrapolation; Depth migration**\*Corresponding author:**Jiachun You  
(youjiachun@cdut.edu.cn)**Citation:** Hu S, Sun P, Li S, Hu F, Guan M, You J. Two-way acoustic wave-equation-based wavefield depth extrapolation for imaging in vertically transversely isotropic media. *J Seismic Explor.* 2026;35(2):025500124.  
doi: 10.36922/JSE025500124**Received:** December 9, 2025**Revised:** February 7, 2026**Accepted:** February 7, 2026**Published online:** April 27, 2026**Copyright:** © 2026 Author(s). This is an Open-Access article distributed under the terms of the Creative Commons Attribution License, permitting distribution, and reproduction in any medium, provided the original work is properly cited.**Publisher's Note:** AccScience Publishing remains neutral with regard to jurisdictional claims in published maps and institutional affiliations.

## 1. Introduction

In seismic exploration and geophysical imaging, the influence of medium anisotropy on wavefield propagation is non-negligible and complicated. Alkhalifah<sup>1,2</sup> demonstrated that velocity anisotropy is pervasive in subsurface formations, with vertically transversely isotropic (VTI) media being particularly dominant in practical exploration settings. Therefore, accurately accounting for VTI characteristics during seismic wavefield modeling, migration, and inversion is critical for improving imaging resolution and positioning accuracy. Over the past few decades, numerous numerical methods and imaging strategies developed for VTI media have been introduced, yielding significant progress. From a comprehensive perspective, Li and Qu<sup>3</sup> reviewed the development of seismic imaging, summarizing the transition from stacking- and migration-based methods to inversion-driven high-resolution approaches and highlighting the role of advanced techniques in complex media.

The accurate imaging of seismic data in VTI media remains a critical topic due to the prevalence of anisotropy in sedimentary basins. Duveneck *et al.*<sup>4</sup> derived a system of first-order acoustic wave equations specifically designed for VTI media and applied it to reverse-time migration (RTM), demonstrating reliable amplitude preservation and robustness against density variations. However, conventional acoustic approximations often suffer from instability, especially in the absence of shear-wave velocity. Bube *et al.*<sup>5</sup> highlighted that such approximations can lead to time-growing instabilities in second-order formulations, which necessitated the development of more stable wavefield propagation schemes. Zhou *et al.*<sup>6</sup> proposed a simplified anisotropic acoustic wave equation for VTI media by decomposing the fourth-order differential equation into a coupled lower-order system via an auxiliary function, facilitating implementation while retaining physical meaning.

To more effectively mitigate P/S wave crosstalk in VTI media, various wave-mode separation techniques have been developed. Yan and Sava<sup>7</sup> proposed pseudo-derivative operators constructed from polarization vectors obtained via the Christoffel equation, enabling effective elastic wavefield decomposition. Zhang and McMechan<sup>8</sup> extended this approach into the wavenumber domain, developing a robust vector decomposition technique for both 2D and 3D elastic wavefields. More recently, Yao *et al.*<sup>9</sup> proposed a pseudo-Helmholtz decomposition operator that leverages wavefront phase direction and eigensystem analysis, offering both computational efficiency and improved mode separation precision. Sun *et al.*<sup>10</sup> introduced a pure qP-wave RTM method using

an elliptical decomposition vector equation, effectively addressing instability and crosstalk issues in VTI media. Shan *et al.*<sup>11</sup> introduced a least-squares Gaussian beam migration method for VTI media, addressing anisotropic effects and improving resolution and amplitude fidelity. Li *et al.*<sup>12</sup> proposed a generalized two-way phase shift operator for acoustic wave-equation depth migration, enhancing subsurface imaging in VTI media. Qin *et al.*<sup>13</sup> proposed a new pure quasi-P wave equation for VTI media, using optical flow to accurately calculate wave propagation directions and correct for anisotropic effects in RTM. Zhang *et al.*<sup>14</sup> extended RTM to VTI media with irregular surfaces, incorporating a boundary-fitted grid to improve imaging accuracy.

Regarding wavefield extrapolation and numerical modeling, low-rank symbol approximation methods have gained popularity. Fomel *et al.*<sup>15</sup> presented a decomposition method in the space-wavenumber domain, which greatly improved the computational efficiency of wavefield propagation in anisotropic media. Sun and Sun<sup>16</sup> further incorporated De Wolf approximation and VTI-generalized screen operators, mitigating aliasing artifacts and enhancing imaging accuracy for complex VTI structures. To account for attenuation effects, Mao *et al.*<sup>17</sup> formulated a viscoacoustic wave equation using complex dispersion relations, combined with the hybrid finite-difference and low-rank decomposition algorithm, accurately modeling qP-wave propagation and dissipation. Similarly, Liang *et al.*<sup>18</sup> developed a decoupled qP-wave equation specifically for VTI media, effectively suppressing artificial qSV-wave dispersion and thereby enhancing the numerical stability and accuracy of the wave-mode representation. Bai *et al.*<sup>19</sup> proposed a viscoelastic anisotropic wave equation for VTI media that decouples dissipation and dispersion, restoring time symmetry via adjusted dissipation terms to improve time-reversal imaging fidelity. Qu *et al.*<sup>20</sup> proposed a Q-compensated least-squares RTM method with velocity-anisotropy correction based on first-order velocity-pressure equations, demonstrating improved deep imaging resolution and amplitude preservation in VTI-attenuating media. Wang *et al.*<sup>21</sup> derived a fractional Laplacian viscoelastic wave equation for VTI-attenuating media, enabling accurate modeling of frequency-independent Q with high computational efficiency.

On the inversion front, advances in full-waveform and reflection-based techniques have enabled more reliable recovery of anisotropic parameters. Wu *et al.*<sup>22</sup> accelerated reflection waveform inversion in acoustic VTI media by integrating second-order adjoint-state methods with a matrix-free Gauss-Newton approach. Singh *et al.*<sup>23</sup> introduced geologically constrained elastic full-

waveform inversion that integrates rock-physics-informed regularization, significantly alleviating parameter coupling and underdetermination in VTI settings. In a probabilistic framework, Lang *et al.*<sup>24</sup> combined a five-parameter VTI reflection model with Bayesian Markov Chain Monte Carlo inversion, enhancing parameter resolution and uncertainty quantification. Moreover, Wang *et al.*<sup>25</sup> focused on multicomponent inversion using a modified SH-SH wave reflection model, yielding high-resolution estimates of anisotropic shear-wave properties. Kamath and Tsvankin<sup>26</sup> performed sensitivity analysis using Fréchet kernels, elucidating the directional radiation behavior of Thomsen parameters and revealing critical insights into wavefield parameter sensitivity and cross-coupling. Li *et al.*<sup>27</sup> analyzed RTM extended images for VTI media, showing  $\eta$ -related residual moveout is dip-dependent and  $\delta$  errors cause defocusing only laterally, guiding anisotropic tomography. Luo *et al.*<sup>28</sup> proposed a hierarchical prestack inversion scheme for VTI media using exact reflection coefficients, thereby improving parameter estimation via a two-stage linear-nonlinear optimization. With the rapid advancement of deep learning, a new class of imaging approaches based on physics-informed neural networks (PINNs) has emerged in recent years. Song *et al.*<sup>29</sup> proposed employing PINNs to model the transmission of acoustic waves in VTI media.

To address the challenges of seismic imaging in anisotropic media, researchers have extensively worked on designing and improving one-way wave-equation depth-imaging techniques tailored to such complex media. Ristow<sup>30</sup> pioneered a finite-difference-based one-way depth-migration method tailored for transversely isotropic media. Building on this foundation, Han and Wu<sup>31</sup> introduced a dual-domain one-way propagator specifically designed for VTI media, enhancing wavefield extrapolation accuracy. Bale<sup>32</sup> proposed a migration technique based on the anisotropic acoustic wave equation, utilizing a phase-shift operator obtained from an adjusted dispersion relation. Fei and Liner<sup>33</sup> extended the hybrid Fourier-finite-difference (Fourier-FD) operator to a 3D depth migration framework, offering improved modeling capabilities for complex anisotropic structures. Bakker<sup>34</sup> developed a more stable one-way propagator for VTI media using a four-way splitting Fourier-FD method. Amazonas *et al.*<sup>35</sup> proposed a hybrid finite-difference operator based on complex Padé approximations, demonstrating enhanced stability for steeply dipping reflectors and effectively reducing migration artifacts. Salcedo *et al.*<sup>36</sup> optimized Padé coefficients to construct a wide-angle continuation operator with improved velocity dependence. Liu and Zhang<sup>37</sup> refined the operator coefficients in the wide-angle regime and incorporated a phase-shift mechanism

to improve imaging precision in VTI media. Vyas *et al.*<sup>38</sup> explored high-resolution one-way wave propagation in tilted transversely isotropic media, thereby expanding the applicability of such methods. Alshuhail and Verschuur<sup>39</sup> proposed a robust migration strategy for VTI media that incorporates internal multiples through a generalized one-way phase-shift operator, thereby improving the reliability of anisotropic parameter estimation via joint migration inversion.

In the context of seismic imaging in anisotropic media, two-way wave-equation-based extrapolation has received increased attention due to its inherent ability to accurately simulate full wavefield behavior.<sup>40–44</sup> This advantage is particularly critical in VTI media, where strong anisotropy produces significant deviations in phase velocity, ray bending, and reflection moveout that standard acoustic or isotropic assumptions cannot adequately handle. Recent studies have shown that two-way propagators can improve the imaging of complex geological structures, particularly in settings with strong vertical velocity gradients or lateral heterogeneity.<sup>45,46</sup> These motivations collectively demonstrate that extending two-way extrapolation methods from isotropic to VTI media is not only theoretically desirable but also essential for achieving accurate and reliable imaging in anisotropic sedimentary basins.

Despite this progress, limited studies have further explored two-way acoustic wave-equation depth migration for VTI media. The contributions of this study can be summarized as follows. First, we extend the two-way acoustic wave-equation depth extrapolation framework to VTI media by deriving a first-order system that explicitly incorporates anisotropic coefficients, enabling accurate wavefield continuation in VTI environments. Second, we introduce a frequency-wavenumber (FK)-domain pseudo-S-wave suppression strategy that eliminates evanescent and spurious wave modes generated during two-way extrapolation, significantly improving the physical fidelity of the propagated P-wavefield. Third, inspired by recent advances in up-down wavefield decomposition, we formulate a separation operator tailored to the VTI two-way framework, enabling stable imaging conditions that reduce low-frequency artifacts. Finally, through comprehensive numerical experiments—including a three-layer model, the Hess model, the Marmousi model, and real land data—we demonstrate that the proposed method consistently outperforms conventional acoustic migration by producing clearer structures, enhanced reflector continuity, and reduced dispersion artifacts. These innovations collectively establish a robust and practical two-way VTI imaging methodology that advances the

current state of anisotropic seismic imaging.

## 2. Methodology

In heterogeneous media, numerical simulation of the elastic wave equation involves solving a coupled system (two components in 2D and three in 3D) relating to the vector elements of the wavefield. The computational cost of propagating each component is comparable to that in the acoustic case, but elastic modeling imposes additional demands on data handling, including the input, output, and storage of wavefield components alongside their corresponding elastic parameters. Unlike the acoustic formulation, which yields only compressional (P) waves, the elastic solution inherently includes both P- and shear (S) waves. This simultaneous propagation of multiple wave modes, while more complete physically, can be inefficient and less targeted for applications focused solely on P-wave modeling and imaging. Alkhalifah<sup>2</sup> introduced an acoustic wave equation specific to VTI media to address this problem, which can be expressed as follows:

$$\frac{\partial^2 p}{\partial t^2} = (1 + 2\eta)v_n^2 \frac{\partial^2 p}{\partial x^2} + v_p^2 \frac{\partial^2 p}{\partial z^2} - 2\eta v_n^2 v_p^2 \frac{\partial^4 F}{\partial x^2 \partial z^2} \quad (1)$$

where  $F(x, z, t) = \int_0^t \int_0^t p(x, z, \tau) d\tau d\tau$ ,  $v_n$  and  $v_p$  are the normal moveout (NMO) and compressional velocities, respectively,  $p$  is the pressure wavefield,  $\varepsilon = \frac{C_{11} - C_{33}}{2C_{33}}$ ,  $\delta = \frac{(C_{13} + C_{44})^2 - (C_{33} - C_{44})^2}{2C_{33}(C_{33} - C_{44})}$ ,  $\eta = \frac{\varepsilon - \delta}{1 + 2\delta}$ ,  $v_n = v_p \sqrt{1 + 2\delta}$ , and the coefficients  $C_{11}$ ,  $C_{33}$ ,  $C_{44}$ , and  $C_{13}$  represent equivalent stiffness parameters in the acoustic VTI approximation, introduced to characterize P-wave propagation and anisotropic effects.

It is noted that **Equation 1** is an acoustic wave equation with  $\eta = 0$ . The space-frequency domain of **Equation 1** can be written as:

$$\omega^2 p + (1 + 2\eta)v_n^2 \frac{\partial^2 p}{\partial x^2} + v_p^2 \frac{\partial^2 p}{\partial z^2} - \frac{2\eta v_n^2 v_p^2}{\omega^2} \frac{\partial^4}{\partial x^2 \partial z^2} p = 0 \quad (2)$$

**Equation 1** represents a second-order partial differential equation in the depth variable  $z$ ; its equivalent first-order partial differential form can be expressed as follows:

$$\frac{\partial P}{\partial z} = WP \quad (3)$$

where  $P = \begin{bmatrix} p \\ p_z \end{bmatrix}$ ,  $W = \begin{bmatrix} 0 & I \\ H & 0 \end{bmatrix}$ , and  $H = \frac{\omega^4 + \omega^2(1 + 2\eta)v_n^2 \frac{\partial^2}{\partial x^2}}{\omega^2 v_p^2 - 2\eta v_n^2 v_p^2 \frac{\partial^2}{\partial x^2}}$ .

**Equation 1** describes the acoustic VTI system in a second-order form, but direct numerical implementation is challenging due to the coupling between temporal and

spatial derivatives. Therefore, we converted it into the first-order system shown in **Equation 3**, which enables wavefield extrapolation in the depth direction. This first-order formulation provides two important benefits: (i) it allows explicit eigenvalue decomposition of the system matrix, enabling separation of downward- and upward-propagating components; and (ii) it facilitates the construction of stable numerical schemes suitable for both forward and backward propagation.

The eigendecomposition of  $W$  is presented as follows:

$$W = \frac{1}{2} \begin{bmatrix} I & I \\ \Lambda & -\Lambda \end{bmatrix} \begin{bmatrix} \Lambda & \\ & -\Lambda \end{bmatrix} \begin{bmatrix} I & \Lambda^{-1} \\ I & \Lambda^{-1} \end{bmatrix} \quad (4)$$

where  $I$  is the identity matrix;  $\Lambda$  is the eigenvalue of matrix  $W$ , with  $\Lambda = ik_z$ ; and  $k_z = \sqrt{H}$  is the vertical wavenumber in VTI media.

The mathematical solution to **Equation 4** within VTI media, for the wavefield depth extrapolation, is presented as follows:

$$P(z_j) = e^{W(z_j - z_i)} P(z_i) \quad (5)$$

where  $P(z_j) = \begin{bmatrix} \tilde{p}(z_j) \\ \tilde{p}_z(z_j) \end{bmatrix}$  is the pressure and its derivative wavefield at depth  $z_j$  levels, and  $P(z_i) = \begin{bmatrix} \tilde{p}(z_i) \\ \tilde{p}_z(z_i) \end{bmatrix}$  is the pressure and its derivative wavefield at depth  $z_i$  levels.

Furthermore, **Equation 3** can be calculated as:

$$\begin{bmatrix} \tilde{p}(z_j) \\ \tilde{p}_z(z_j) \end{bmatrix} = \begin{bmatrix} \cos(k_z \Delta z) & \frac{\sin(k_z \Delta z)}{k_z} \\ -k_z \sin(k_z \Delta z) & \cos(k_z \Delta z) \end{bmatrix} \begin{bmatrix} \tilde{p}(z_i) \\ \tilde{p}_z(z_i) \end{bmatrix} \quad (6)$$

where  $\Delta z = z_i - z_j$ .

A key challenge in using two-way extrapolation in VTI media is the generation of pseudo-S-waves—artificial modes that arise from the acoustic approximation but do not correspond to any physically meaningful propagation. If not properly suppressed, these modes contaminate the extrapolated wavefield and introduce significant migration artifacts. In this study, we integrated an FK-domain filter based on the sign properties of the dispersion relation (Section A1), ensuring that only wave components associated with positive P-wave propagation are retained<sup>32</sup>.

Because the proposed scheme performs wavefield depth extrapolation using a two-way wave equation, low-frequency artifacts are produced when using a cross-correlation imaging condition for the source and receiver wavefields. Therefore, the up- and down-going wavefields for source and receiver data need to be separated. Inspired by You *et al.*<sup>42</sup>, a new pressure wavefield  $q$  is defined as:



$$\tilde{q} = \frac{\tilde{p}}{ik_z} \quad (7)$$

Based on **Equation 6**, the novel wavefield depth extrapolation method can be formulated as follows:

$$\begin{bmatrix} \tilde{p}(z_i) \\ \tilde{q}(z_i) \end{bmatrix} = \begin{bmatrix} \cos(k_z \Delta z) & i \sin(k_z \Delta z) \\ i \sin(k_z \Delta z) & \cos(k_z \Delta z) \end{bmatrix} \begin{bmatrix} \tilde{p}(z_i) \\ \tilde{q}(z_i) \end{bmatrix} \quad (8)$$

By using **Equation 7**, the up- and down-going wavefields can be further derived as:

$$\begin{cases} \tilde{p}_d = \frac{1}{2}[\tilde{p} + \tilde{q}] \\ \tilde{p}_u = \frac{1}{2}[\tilde{p} - \tilde{q}] \end{cases} \quad (9)$$

where  $\tilde{p}_d$  and  $\tilde{p}_u$  are the up- and down-going wavefields, respectively.

During each depth extrapolation, the conventional imaging result can be achieved using wavefield separation based on **Equation 9**, and can be expressed as:

$$Image = \sum_{\omega} \tilde{p}_s^d \cdot \tilde{p}_r^{u*} \quad (10)$$

where  $\tilde{p}_s^d$  and  $\tilde{p}_r^u$  represent the down-going source wavefield and up-going receiver wavefield, respectively, and \* denotes the conjugate operator.

Based on the above algorithm description, the specific

implementation is shown in [Table 1](#).

### 3. Results

To comprehensively evaluate the performance of the proposed VTI two-way extrapolation method, we designed numerical experiments spanning a range of geological complexities—from layered media to strongly faulted structures and real field data situations. The goal of these tests is not only to validate the numerical stability of the method but also to demonstrate its advantages in resolving phase dispersion, maintaining reflector continuity, and preserving amplitude relative to conventional acoustic migration.

#### 3.1. Three-layer model

A three-layer synthetic model, illustrated in [Figure 1](#), was constructed with spatial dimensions of 3,000 m in depth (z) and 6,000 m in width (x). The grid sampling intervals were set to 10.0 m vertically and 20.0 m horizontally. A Ricker wavelet centered at 20.0 Hz served as the source function. Seismic data acquisition spanned 2.0 s with a temporal sampling rate of 0.001 s. Receivers were uniformly placed along the surface from 0 to 6,000 m at 20.0 m intervals. Additionally, 150 shot points were arranged with a spacing of 40.0 m.

The simulated shot gathers for both acoustic and VTI media are shown in [Figure 2](#). At a representative location (x = 1,000 m), the waveform response in the VTI medium exhibited pronounced phase dispersion

**Table 1. Two-way vertically transversely isotropic wavefield depth extrapolation and imaging**

Category	Description
Input	Acoustic VTI model parameters $v_{nmo}(x, z)$ , $v_p(x, z)$ , anisotropic parameters $\varepsilon(x, z)$ , $\delta(x, z)$ ; Source wavelet $s(t)$ ; Recorded seismic data $d(x_r, t)$ ; Depth step $\Delta z$ ; Frequency sampling $\omega$ .
Steps	1) Initialization: Transform the source wavelet and recorded seismic data from the time domain to the frequency domain. Initialize the source and receiver wavefields at the surface depth $z = 0$ ; Depth extrapolation: For each depth step, extrapolate both source and receiver wavefields downward using the two-way wavefield extrapolation operator ( <b>Equation 6</b> ); Pseudo-S-wave and evanescent-wave suppression: Apply a frequency–wavenumber-domain filter to the extrapolated wavefields to remove pseudo-S-wave and evanescent components based on the dispersion relation criteria (Section A1); Wavefield transformation: Compute the auxiliary pressure wavefield using <b>Equation 7</b> to facilitate stable separation of wavefield components; Up- and down-going wavefield separation: Decompose the source and receiver wavefields into down-going and up-going components using <b>Equation 9</b> ; Imaging condition: Apply the cross-correlation imaging condition by correlating the down-going source wavefield with the up-going receiver wavefield at each depth level ( <b>Equation 10</b> ); Image accumulation: Sum the imaging contributions over all frequencies and shots to obtain the final migrated image $I(x, z)$ .
Output	Depth-domain migrated image $I(x, z)$ .

relative to its acoustic counterpart, as seen in Figure 2C. An enlarged view of the region highlighted by the red-dashed rectangle in Figure 2C is shown in Figure 2D to more clearly illustrate the phase discrepancies. Using these VTI data, both a conventional acoustic migration and the proposed VTI-based migration method were performed. Figure 3 presents the resulting images. The conventional acoustic approach produced a structurally correct image but exhibited significant phase-dispersion artifacts in imaging results. In contrast, the VTI scheme yielded a more coherent image with minimal dispersion artifacts.

In the three-layer example, the model was intentionally kept simple to clearly observe the influence of VTI anisotropy. By comparing the acoustic and VTI shot gathers, we observed systematic phase discrepancies originating from directional velocity differences introduced by  $\epsilon$  and  $\delta$ . These discrepancies propagated directly into the migration results: the acoustic scheme yielded smeared reflectors, while the VTI scheme reconstructed sharper interfaces. This example highlights the fundamental necessity of anisotropy correction even in structurally simple environments.

### 3.2. Hess model

An anisotropic Hess model was used for imaging comparison, as shown in Figure 4, with a vertical extent of 2,500 m and a horizontal span of 10,000 m. The spatial sampling intervals were set to 10.0 m in the vertical direction and 20.0 m horizontally. The source was represented by a 20.0 Hz Ricker wavelet. Data acquisition spanned 3.0 s with samples recorded every 0.001 s. Receivers were positioned uniformly along the surface from 0 to 10,000 m at 20.0 m

intervals, while 250 shot points were placed every 40.0 m.

Modeled shot gathers for acoustic and VTI media are displayed in Figure 5. At  $x = 6,000$  m, the VTI simulation revealed significant phase dispersion compared to the acoustic case, as shown in Figure 5C. Figure 5D zooms into the region outlined by the red-dashed rectangle in Figure 5C, providing a clearer view of the phase variation between the two media. To assess migration accuracy, both the proposed VTI method and the conventional acoustic approach were applied to data generated from VTI models. As illustrated in Figure 6, the VTI migration produces clearer, more geologically consistent images with fewer artifacts and improved structural continuity, as indicated by the red-dashed ellipse. For the Hess VTI model, which contained strong lateral velocity gradients and dipping structures, the advantage of the proposed method became more pronounced. Acoustic migration visibly distorted reflectors beneath high-velocity regions, particularly in areas with strong anisotropy. The proposed VTI method significantly improved the continuity of deep reflectors and reduced migration noise in the model's flanks, as highlighted by the red arrows in Figure 6. The improvement in imaging accuracy was not only quantitative but also qualitative in regions that were typically difficult for one-way acoustic methods to handle.

### 3.3. Marmousi model

The anisotropic Marmousi model, shown in Figure 7, spanned 2,000 m in depth and 8,000 m in width, with vertical and horizontal sampling intervals of 10.0 m and 20.0 m, respectively. A Ricker wavelet centered at 20.0 Hz was used to excite the model. Seismic recordings extended

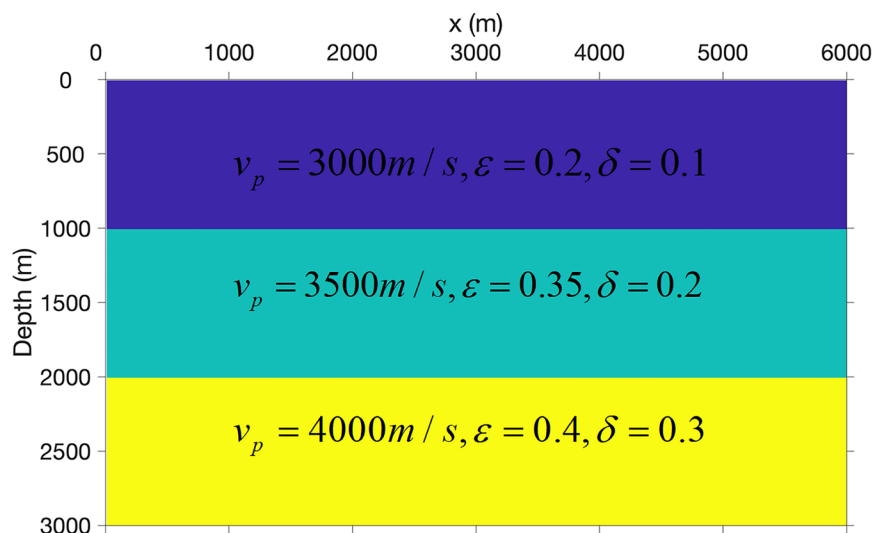
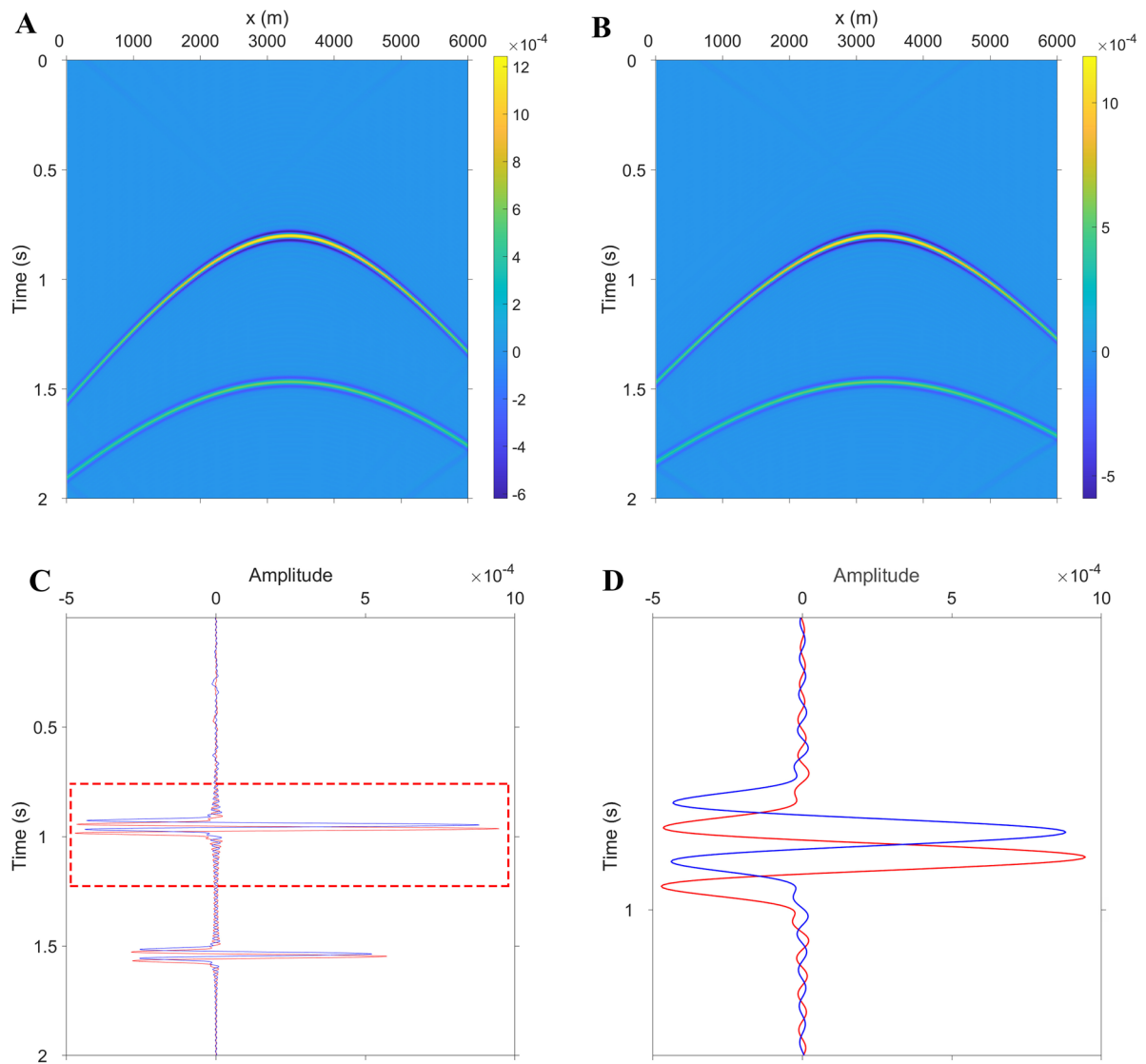
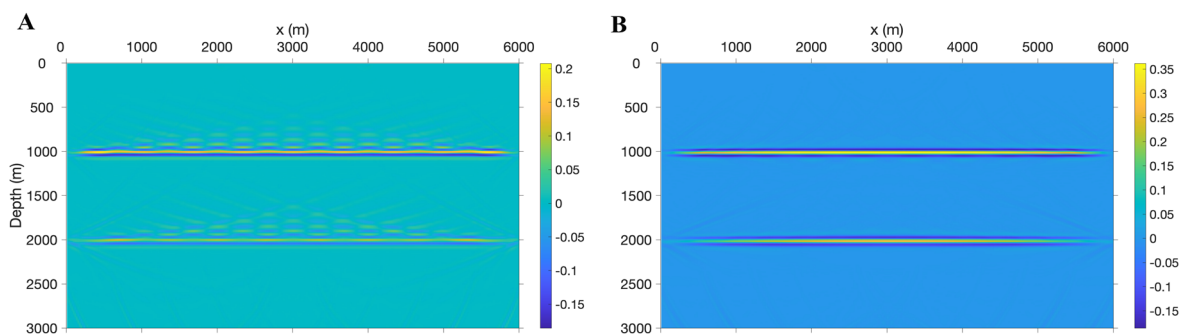


Figure 1. Anisotropy parameters of the three-layer model



**Figure 2.** Shot gather obtained in (A) acoustic media and (B) vertically transversely isotropic (VTI) media. (C) Waveform comparison. (D) Enlarged view of the area highlighted by the red-dashed rectangle in (C). The red line denotes waveforms calculated in acoustic media, while the blue line presents waveforms calculated in VTI media.



**Figure 3.** Imaging results of shot gathers obtained from (A) acoustic media and (B) vertically transversely isotropic media

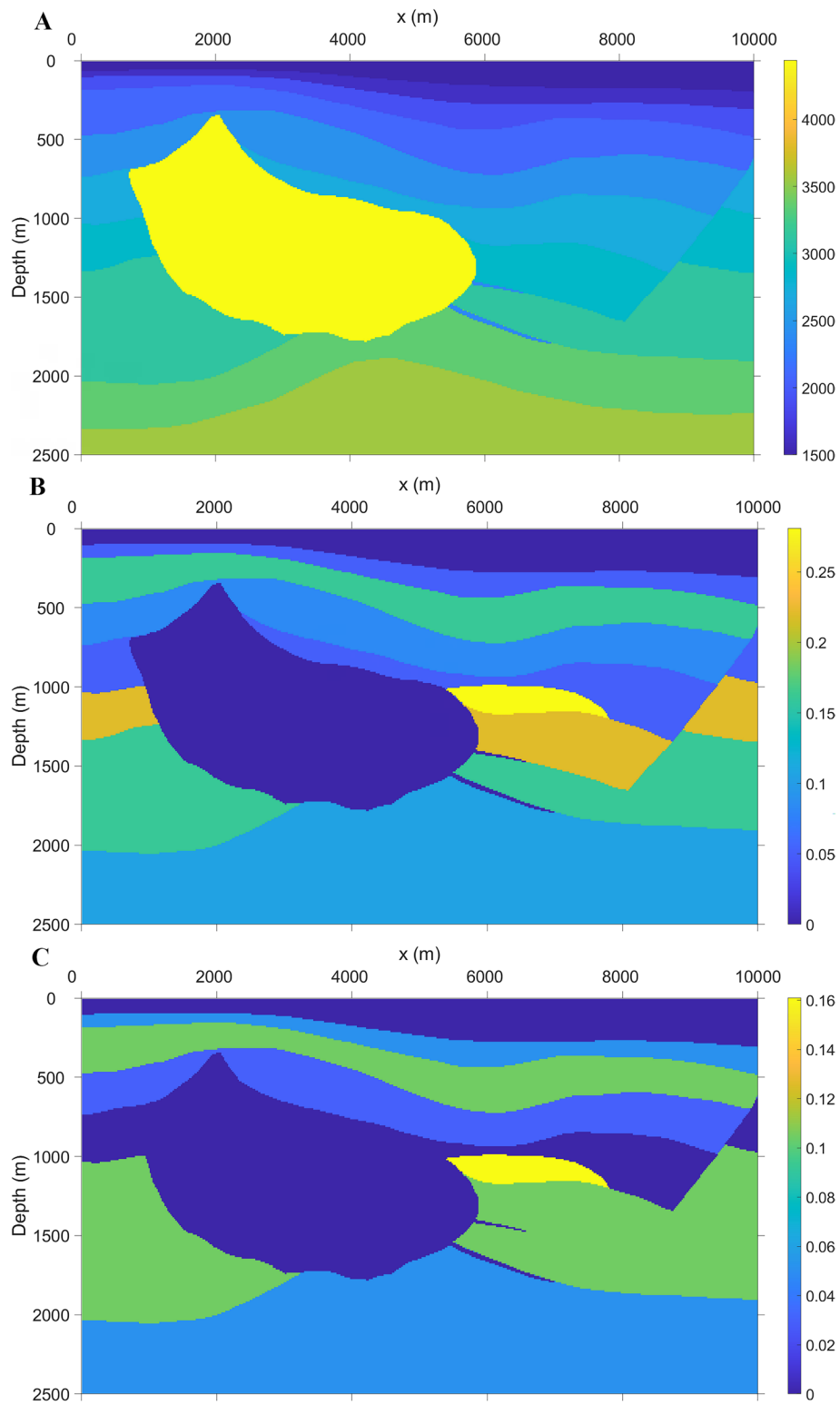


**Figure 4.** Hess model parameters: (A) P-wave velocity, (B) anisotropy parameter  $\epsilon$ , and (C) anisotropy parameter  $\delta$

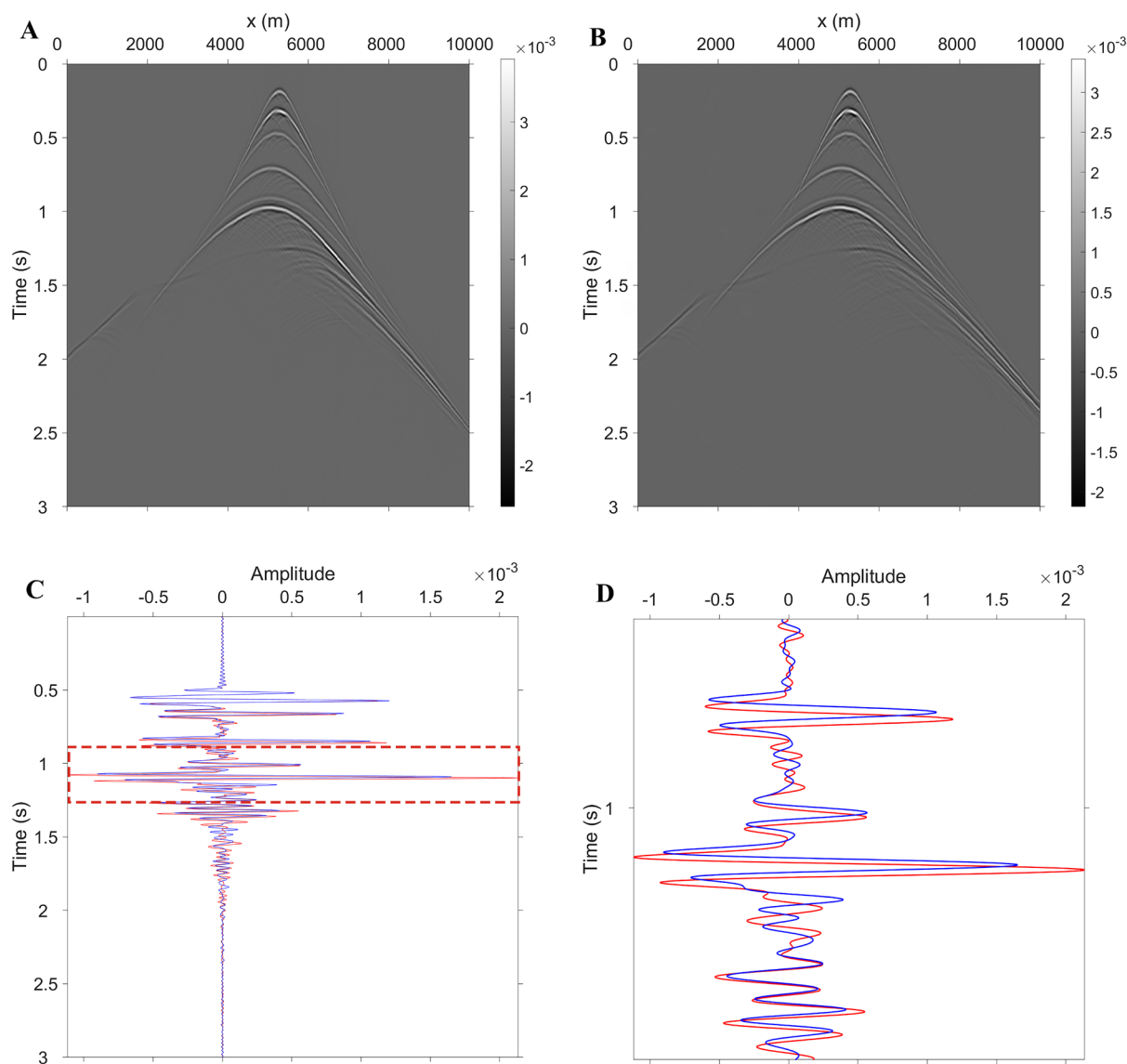


**Figure 5.** Shot gathers obtained from (A) acoustic media and (B) vertically transversely isotropic (VTI) media. (C) Waveform comparison. (D) Enlarged view of the area highlighted by the red-dashed rectangle in (C). The red line denotes waveforms calculated in acoustic media, while the blue line presents waveforms calculated in VTI media.

to 3.0 s with a temporal resolution of 0.001 s. The receiver array covered the entire model top from 0 to 8,000 m with a 20.0 m spacing, and 200 shot points were distributed at 40.0 m spacing.

Figure 8 illustrates the shot gathers for both acoustic and VTI conditions. At  $x = 5,000$  m, the VTI medium again displayed clear phase dispersion, in contrast to the acoustic case, as depicted in Figure 8C. To emphasize the phase differences, an enlarged view of the highlighted region in Figure 8C is provided in Figure 8D, allowing for a more detailed comparison of the waveform behavior

between the two media.

For migration, both the proposed VTI-based method and the conventional acoustic strategy were employed. The resulting images in Figure 9 show that the acoustic scheme failed to resolve complex structures between the three major faults. The Marmousi VTI model further tested the method's ability to recover complex fault geometries and thin-bed structures. The acoustic migration failed to reconstruct reflector terminations between major faults, whereas the VTI method recovered them with greater clarity and consistency, as indicated by the red-dashed

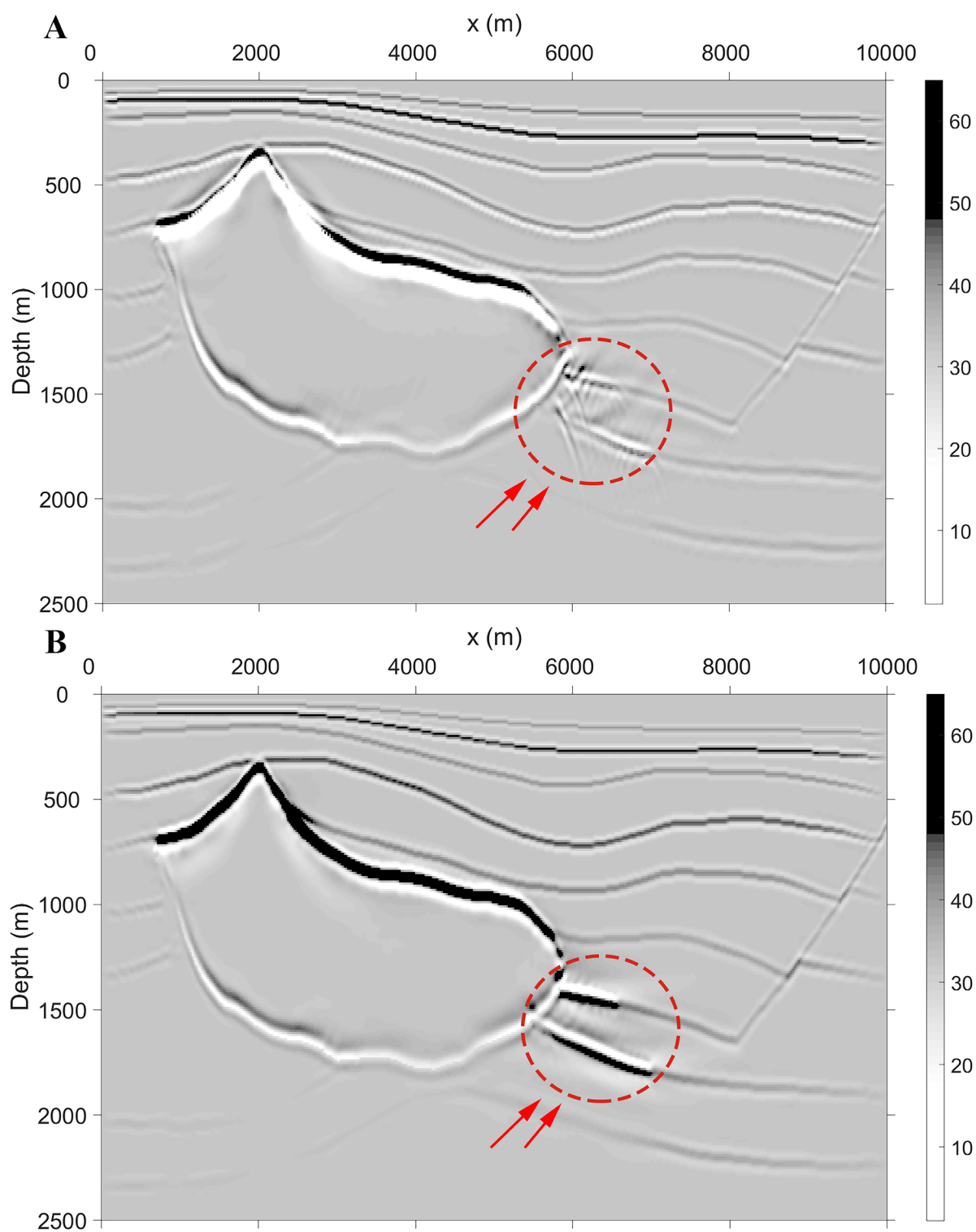


**Figure 6.** Imaging results of shot gather obtained from (A) acoustic media and (B) vertically transversely isotropic media. The red-dashed ellipse and arrows illustrate the imaging differences.



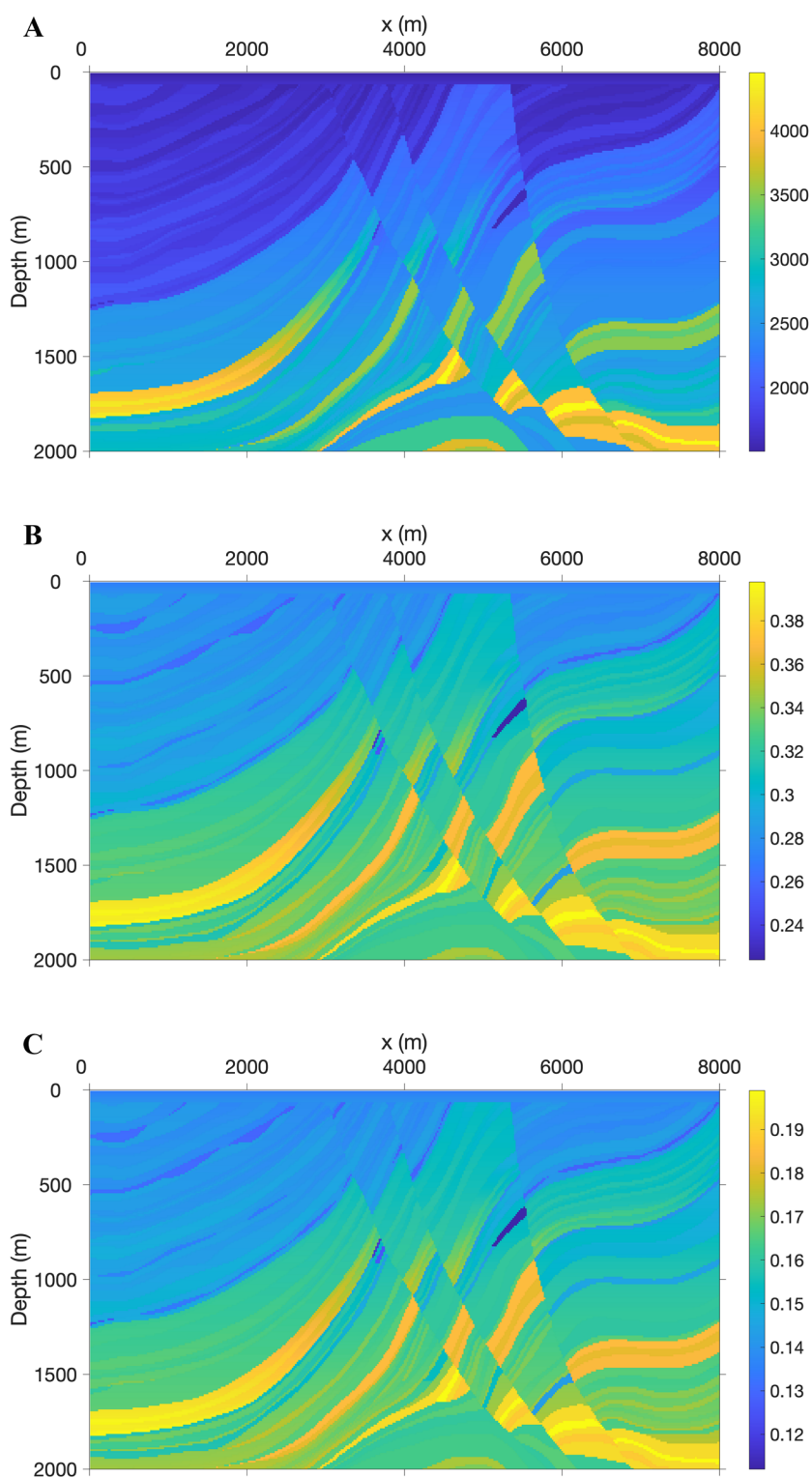


**Figure 7.** Marmousi model parameters: (A) P-wave velocity, (B) anisotropy parameter  $\epsilon$ , and (C) anisotropy parameter  $\delta$

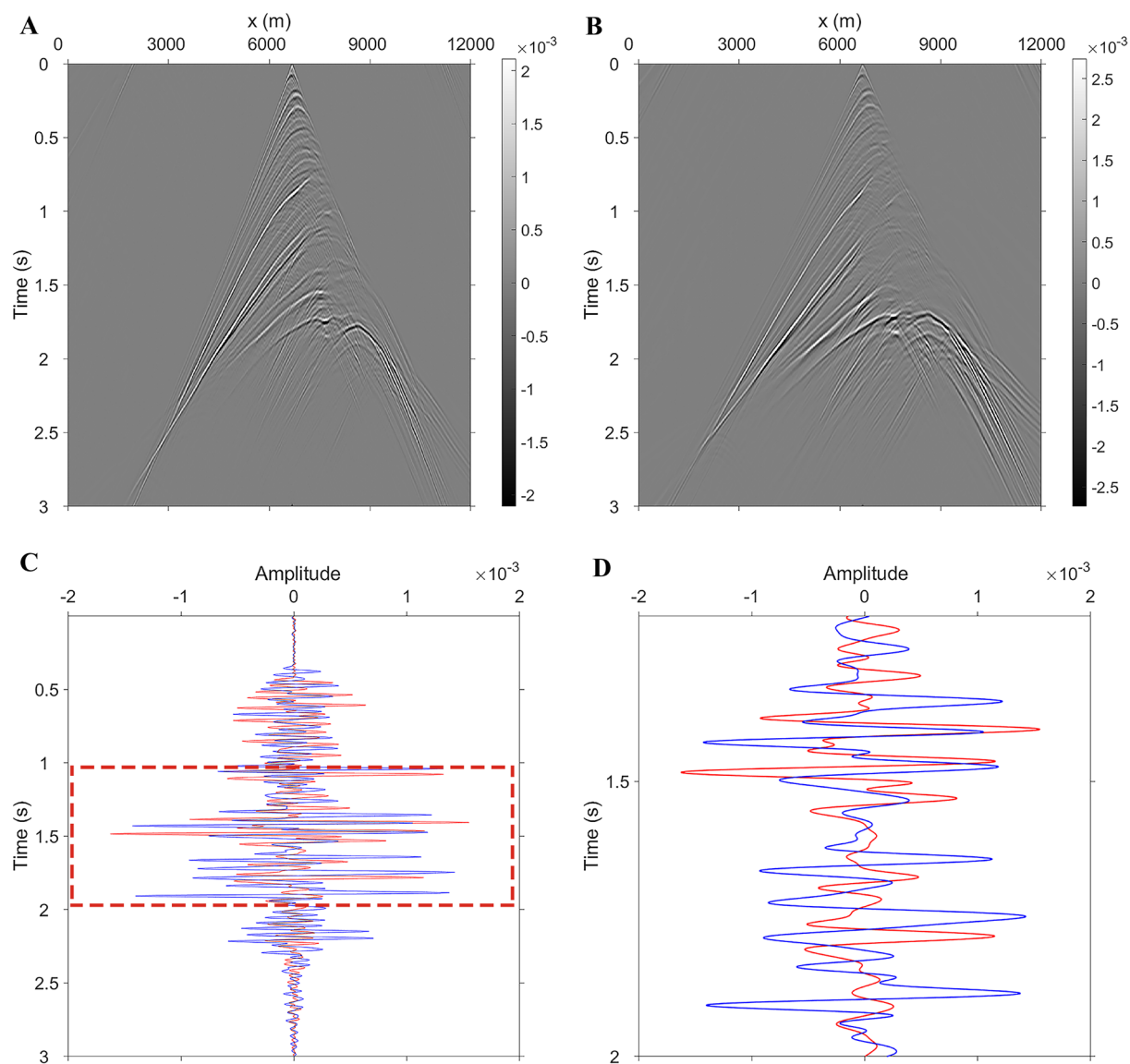


**Figure 8.** Shot gather obtained from (A) acoustic media and (B) vertically transversely isotropic (VTI) media. (C) Waveform comparison. (D) Enlarged view of the area highlighted by the red-dashed rectangle in (C). The red line denotes waveforms calculated in acoustic media, while the blue line presents waveforms calculated in VTI media.

ellipse. These results indicate that the proposed two-way extrapolation can maintain accurate phase propagation even under strong lateral heterogeneity and anisotropic variations. To further highlight local differences, Figure 10 presents zoomed-in views of representative regions. Figure 10A,B correspond to acoustic and VTI media, respectively, demonstrating that the VTI method better preserved reflector continuity and phase characteristics at the small scale.

### 3.4. Real data application

To evaluate the effectiveness of the proposed method on real data, we applied our imaging workflow to a land seismic dataset obtained from previous studies.<sup>47,48</sup> The shot gathers used in this study are shown in Figure 11. As observed from the gathers, the continuity of reflection events was relatively poor, particularly for deeper reflections, which is typical for land data acquired in geologically complex areas.



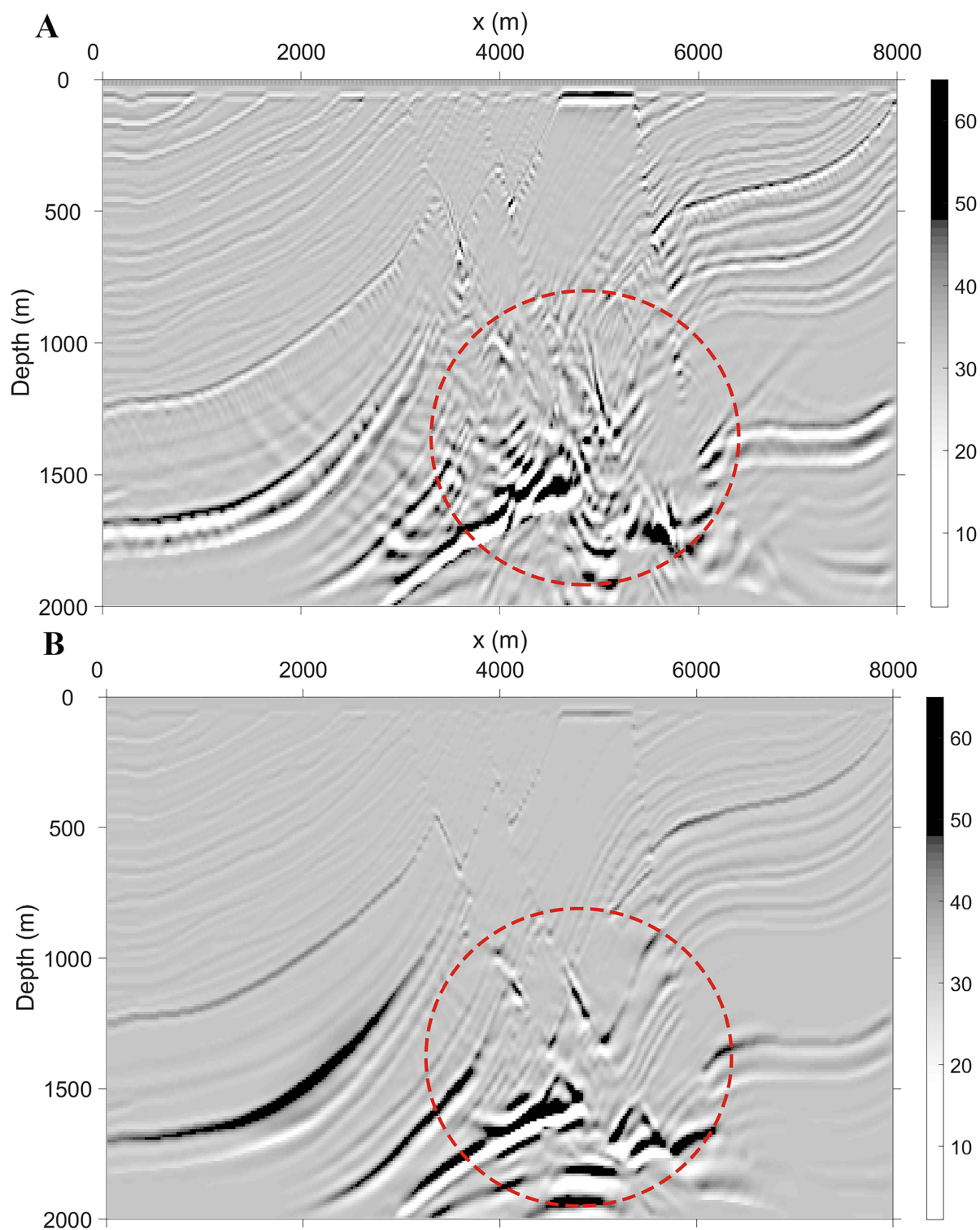


**Figure 9.** Imaging results of shot gather obtained from (A) acoustic media and (B) vertically transversely isotropic media. The red-dashed ellipse shows the imaging differences.

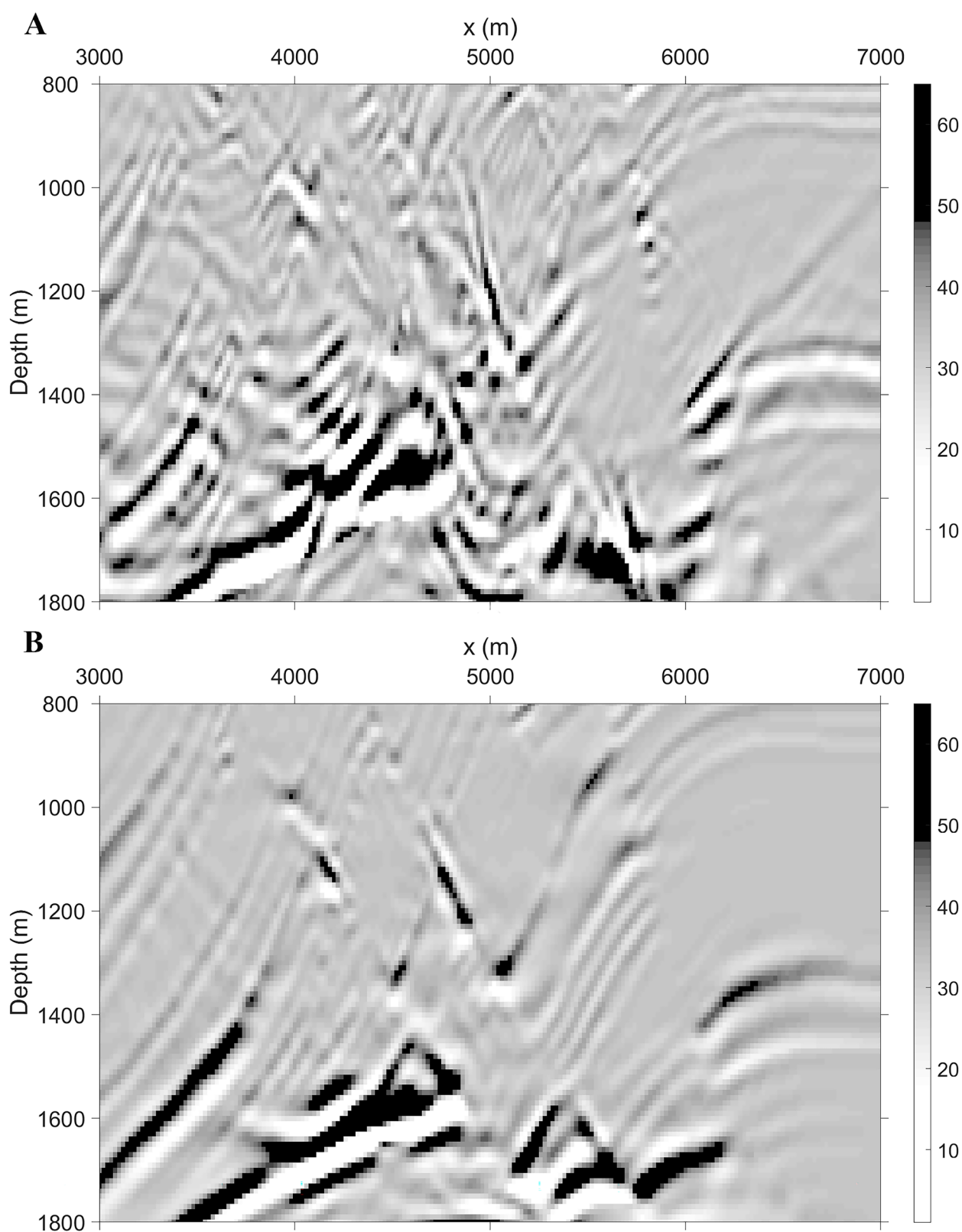


**Figure 10.** Local imaging results from (A) acoustic media and (B) vertically transversely isotropic media

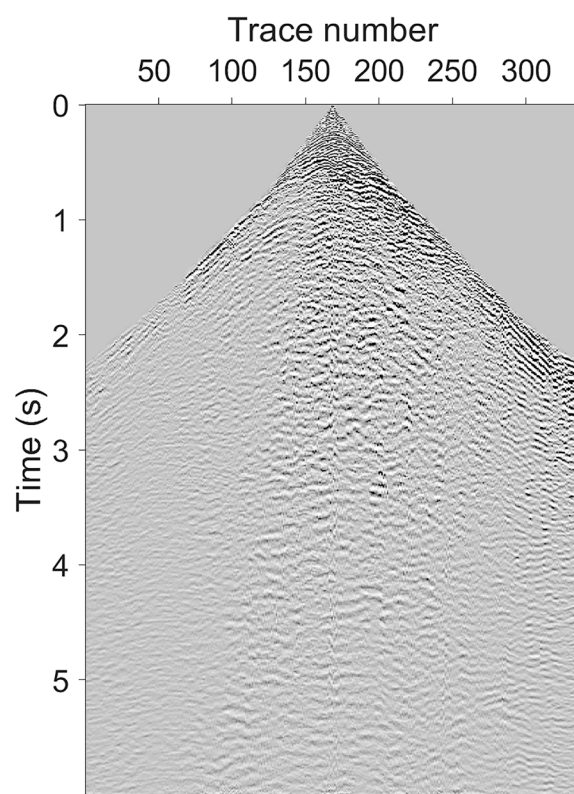


Figure 11. Real land seismic shot gathers

A depth-domain velocity model, together with the corresponding epsilon and delta fields, was constructed using a conventional VTI traveltime inversion scheme (Figure 12).<sup>49,50</sup> Using this model, we performed depth imaging of the shot gathers with two different two-way wave-equation-based migration approaches: one assuming an acoustic (isotropic) medium and the other incorporating VTI anisotropy. The resulting migrated images are presented in Figure 13.

From the perspective of structural imaging, the two-way wave-equation-based migration method for VTI media developed in this study produced a noticeably more coherent and geologically consistent image, as indicated by the red-dashed ellipse. Compared with the acoustic migration result, the VTI migration enhanced the continuity of key structural reflectors, as highlighted by the red arrows in Figure 13. To further illustrate these differences, Figure 14 shows zoomed-in views of the two regions indicated by the red ellipses in Figure 13, where the VTI results exhibited clearer reflector terminations and improved local continuity compared with the acoustic counterparts. The imaging performance on this real land dataset demonstrates the practical advantages of the proposed VTI two-way propagator in resolving subsurface

structures and improving reflector continuity.

#### 4. Discussion

A key novelty of our work lies in the explicit construction of a two-way VTI propagator based on the first-order system derived from the acoustic VTI wave equation. Traditional acoustic depth-migration methods assume isotropy during wavefield extrapolation, leading to phase inaccuracies when applied to anisotropic models. Moreover, the coupling between P- and pseudo-S-wave components becomes particularly problematic when depth extrapolation is performed using two-way equations, because the imaging condition tends to amplify low-wavenumber artifacts. By integrating an FK-domain filtering strategy into the extrapolation process, we successfully eliminated pseudo-S-wave and evanescent-wave energy while retaining the physically meaningful P-wave response. This step is crucial for obtaining stable, interpretable imaging results. It represents a key methodological advancement over classical two-way extrapolation schemes.

Despite these improvements, some limitations remain. First, the current formulation uses an acoustic VTI approximation and therefore does not capture any real shear-wave physics and therefore neglects elastic mode

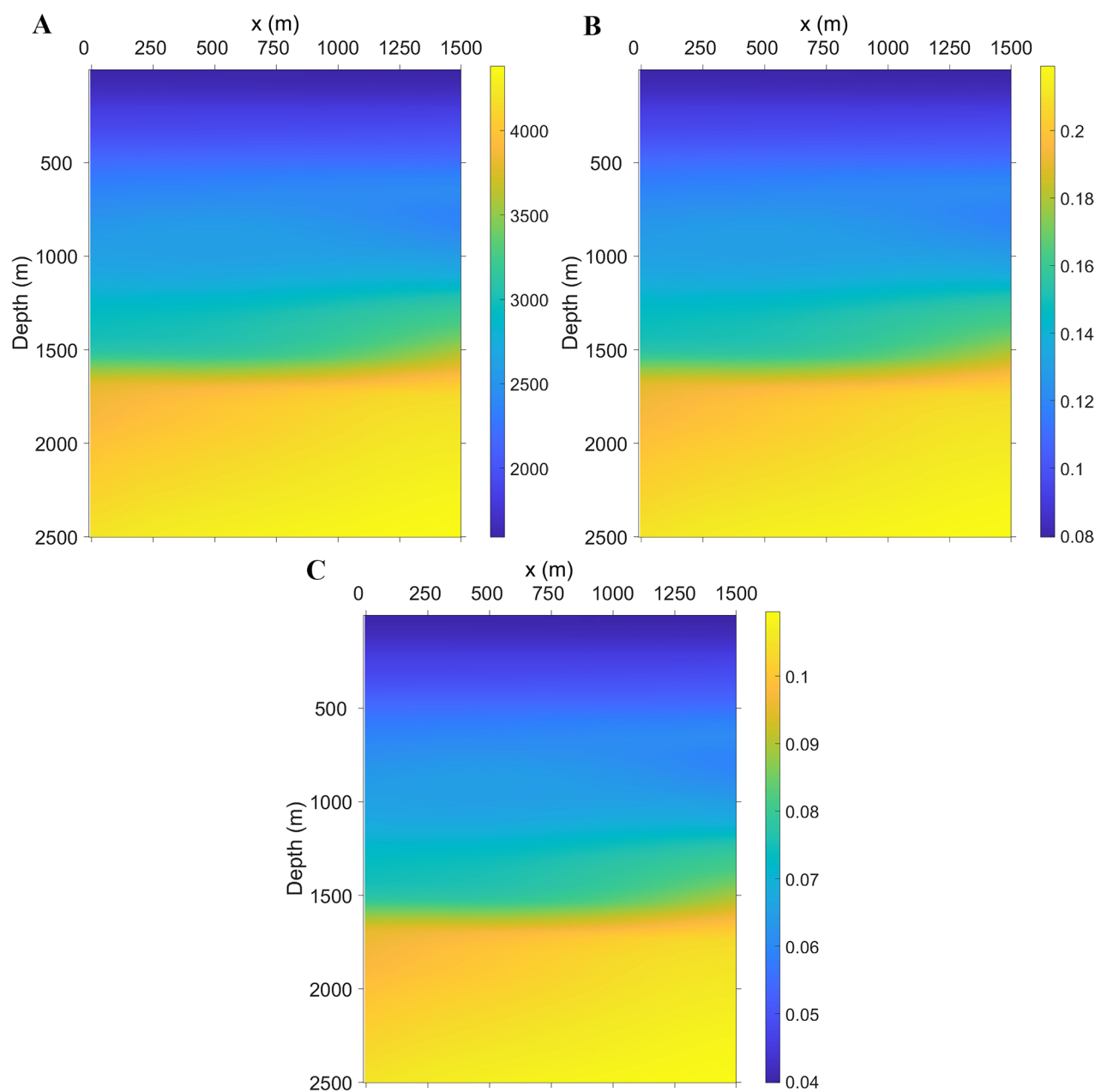


**Figure 12.** Real data parameters: (A) P-wave velocity, (B) anisotropy parameter  $\epsilon$ , and (C) anisotropy parameter  $\delta$

conversions and qS-related responses. While the pseudo-S suppression strategy works well for P-wave imaging, this approximation may limit the method's applicability in areas where elastic effects are non-negligible, and incorporating elastic effects or qSV-sensitive reflections may require extending the method to a fully elastic two-way formulation. Second, the method's accuracy depends heavily on the quality of the anisotropic parameters ( $\epsilon$  and  $\delta$ ), which are often difficult to estimate reliably in practical applications. Errors in anisotropic model

building may propagate into the extrapolated wavefields, degrading imaging performance and potentially leading to residual artifacts and reduced image focusing. Therefore, tighter integration with anisotropic velocity/parameter inversion—such as reflection-based waveform inversion or PINN-based parameter estimation—is essential to improve the method's robustness in field-data applications.

Future research may focus on several aspects. One direction is to generalize the proposed two-way propagator

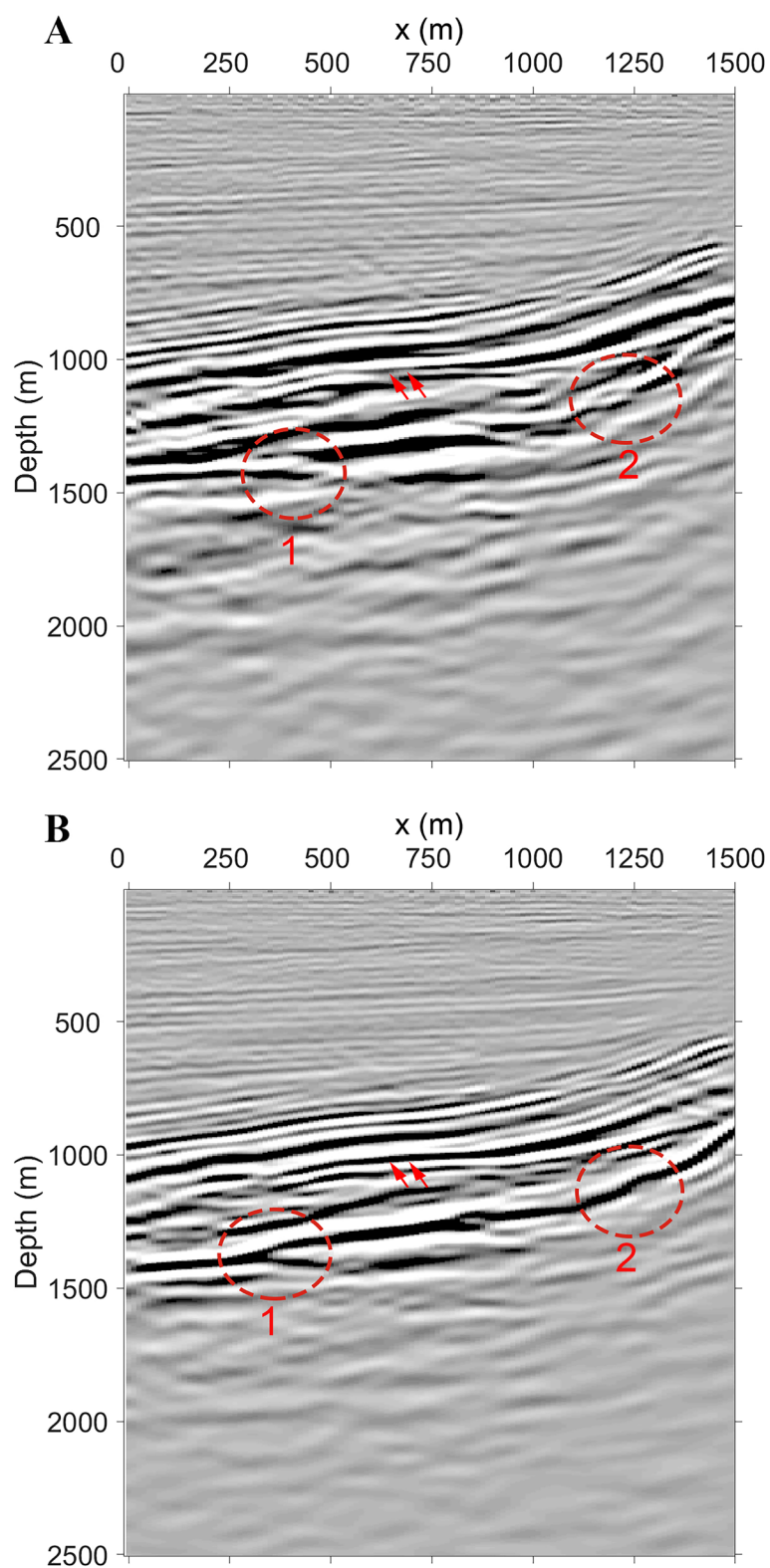


**Figure 13.** Imaging results of shot gather obtained from (A) acoustic media and (B) vertically transversely isotropic media. The red-dashed ellipse and arrows indicate the imaging differences.



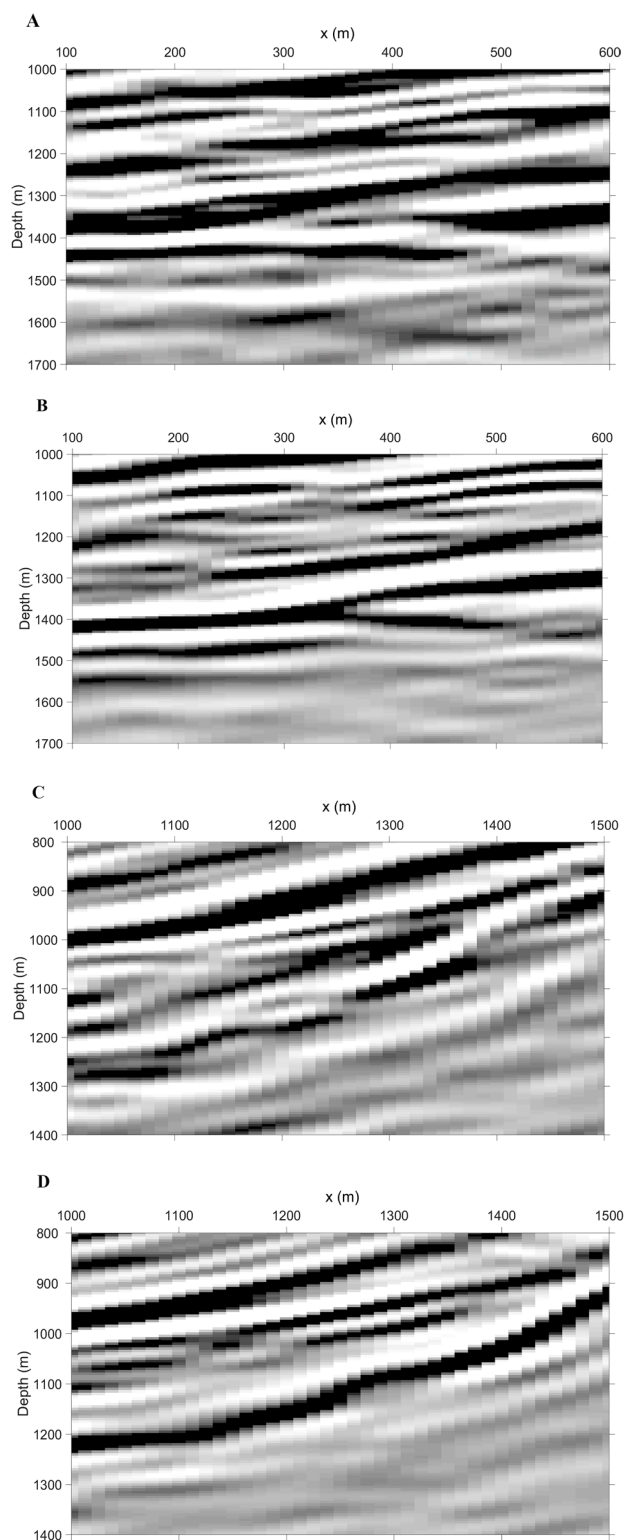


**Figure 14.** Local imaging results for the regions indicated by red ellipses in Figure 13. (A) Red ellipse 1 in Figure 13A. (B) Red ellipse 1 in Figure 13B. (C) Red ellipse 2 in Figure 13A. (D) Red ellipse 2 in Figure 13B.

to tilted-transverse isotropy media, which are often required for imaging complex geologic structures, such as sub-salt regions and thrust belts. Another promising extension is the development of joint velocity and anisotropy estimation workflows based on the proposed two-way operator, potentially using gradient-based inversion or machine-learning-enhanced optimization. Furthermore, combining the proposed propagator with least-squares migration could enhance amplitude fidelity and improve the recovery of weak reflections. Finally, GPU-parallelized implementations may significantly accelerate the computational efficiency of the two-way VTI extrapolation operator, making it more suitable for large-scale industrial applications.

## 5. Conclusion

To address the challenge of accurate seismic imaging in anisotropic media, this study proposed a novel acoustic two-way wave-equation wavefield depth extrapolation method specifically designed for imaging in VTI media. Extensive simulations verified that the proposed VTI imaging strategy, based on the two-way wave equation, consistently outperformed the traditional acoustic approach in processing data from anisotropic media. Across a range of geological scenarios—from a simple three-layer model to the velocity-gradient Hess model and the structurally complex Marmousi model—the conventional acoustic method produced images with notable phase distortion and structural inaccuracies because it could not accommodate anisotropic effects. In contrast, the VTI scheme yielded significantly improved imaging results, effectively suppressing phase dispersion and enhancing structural continuity, particularly in geologically complex regions. These findings underscore the limitations of conventional acoustic assumptions for representing the anisotropic nature of real Earth media and highlight the need for VTI-based methods to achieve high-fidelity seismic imaging.

## Acknowledgments

None.

## Funding

This work was supported by the open research project of the National Engineering Research Center for Oil and Gas Exploration Computer Software (DFWT-ZYRJ-2025-JS-56) and Sichuan Science and Technology Program (2026NSFSC0234, 2024NSFSC0810).

## Conflict of interest

Jiachun You is a Guest Editor of this special issue, but was

not in any way involved in the editorial and peer-review process conducted for this paper, directly or indirectly. The authors declare that they have no known competing financial interests or personal relationships that could have appeared to influence the work reported in this paper.

## Author contributions

*Conceptualization:* Shanzheng Hu

*Formal analysis:* Pengyuan Sun

*Investigation:* Jiachun You

*Methodology:* Jiachun You

*Writing—original draft:* Shuqin Li

*Writing—review & editing:* Feng Hu, Min Guan

## Availability of data

Data will be made available upon request to the corresponding author.

## References

1. Alkhalifah T. Acoustic approximations for processing in transversely isotropic media. *Geophysics*. 1998;63(2):623-631.  
doi: 10.1190/1.1444361
2. Alkhalifah T. An acoustic wave equation for anisotropic media. *Geophysics*. 2000;65(4):1239-1250.  
doi: 10.1190/1.1444815
3. Li ZC, Qu YM. Research progress on seismic imaging technology. *Pet Sci*. 2022;19(1):128-146.  
doi: 10.1016/j.petsci.2022.01.015
4. Duveneck E, Milcik P, Bakker PM, Perkins C. Acoustic VTI wave equations and their application for anisotropic reverse-time migration. In: *SEG Technical Program Expanded Abstracts 2008*; Society of Exploration Geophysicists; 2008:2186-2190.  
doi: 10.1190/1.3059320
5. Bube KP, Nemeth T, Stefani JP, *et al*. On the instability in second-order systems for acoustic VTI and TTI media. *Geophysics*. 2012;77(5):T171-T186.  
doi: 10.1190/geo2011-0250.1
6. Zhou H, Zhang G, Bloor R. An Anisotropic Acoustic Wave Equation for VTI Media. In: *Proceedings of the 68th EAGE Conference and Exhibition Incorporating SPE EUROPEC 2006*; June 12-15, 2006; Vienna, Austria. European Association of Geoscientists & Engineers; 2006:cp-2-00318.  
doi: 10.3997/2214-4609.201402310
7. Yan J, Sava P. Elastic wave-mode separation for VTI media. *Geophysics*. 2009;74(5):WB19-WB32.  
doi: 10.1190/1.3184014

8. Zhang Q, McMechan GA. 2D and 3D elastic wavefield vector decomposition in the wavenumber domain for VTI media. *Geophysics*. 2010;75(3):D13-D26.  
doi: 10.1190/1.3431045
9. Yao G, Fang X, Zheng Q, *et al.* Pseudo-Helmholtz decomposition for an elastic VTI wavefield based on wavefront phase direction. *Geophysics*. 2024;89(3):T151-T162.  
doi: 10.1190/geo2023-0574.1
10. Sun S, Mao W, Zhang Q, *et al.* Reverse-time migration for pure qP-wave based on elliptical decomposition vector equation. *IEEE Trans Geosci Remote Sens*. 2024;62:1-12.  
doi: 10.1109/TGRS.2024.3406763
11. Shan T, Yang J, Huang J, Wang W, Qin S. Least-Squares Gaussian Beam Migration in the VTI Media With a Cauchy Constraint. *IEEE Trans Geosci Remote Sens*. 2025;63:1-9.  
doi: 10.1109/tgrs.2025.3554996
12. Li A, Li C, Lai F, Liao J, Liu T. An Acoustic Wave-Equation Depth Migration Method Using Generalized Two-Way Phase Shift Operator for Anisotropic Media. *IEEE Geosci Remote Sens Lett*. 2025;22:1-5.  
doi: 10.1109/lgrs.2025.3549919
13. Qin S, Yang J, Wang P, Huang J, Qin N. Seismic imaging of pure quasi-P-wave in the VTI media by using the optical flow to calculate phase-velocity direction. *Geophys J Int*. 2025;242(3):ggaf270.  
doi: 10.1093/gji/ggaf270
14. Zhang K, Guo LJ, Li ZC, *et al.* Reverse time migration of VTI media in undulating surface based on the first-order velocity-stress equation. *Geophys Prospect Petr*. 2026;65(1):77-87. [In Chinese].  
doi: 10.12431/issn.1000-1441.2024.0135
15. Fomel S, Ying L, Song X. Seismic wave extrapolation using lowrank symbol approximation. *Geophys Prospect*. 2013;61(3):526-536.  
doi: 10.1111/j.1365-2478.2012.01064.x
16. Sun H, Sun J. A VTI medium prestack migration method based on the De Wolf approximation. *Comput Geosci*. 2025;196:105835.  
doi: 10.1016/j.cageo.2024.105835.
17. Mao Q, Huang JP, Mu XR, *et al.* Accurate simulations of pure-viscoacoustic wave propagation in tilted transversely isotropic media. *Pet Sci*. 2024;21(2):866-884.  
doi: 10.1016/j.petsci.2023.11.005
18. Liang K, Cao D, Sun S, *et al.* Decoupled wave equation and forward modeling of qP wave in VTI media with the new acoustic approximation. *Geophysics*. 2023;88(1):WA335-WA344.  
doi: 10.1190/geo2022-0292.1
19. Bai T, Zhu T, Tsvankin I. Attenuation compensation for time-reversal imaging in VTI media. *Geophysics*. 2019;84(4):C205-C216.  
doi: 10.1190/geo2018-0532.1
20. Qu Y, Zhu J, Chen Z, *et al.* Q-compensated least-squares reverse time migration with velocity-anisotropy correction based on the first-order velocity-pressure equations. *Geophysics*. 2022;87(6):S335-S350.  
doi: 10.1190/geo2021-0689.1
21. Wang N, Xing G, Zhu T, *et al.* Propagating seismic waves in VTI attenuating media using fractional viscoelastic wave equation. *J Geophys Res Solid Earth*. 2022;127(4):e2021JB023280.  
doi: 10.1029/2021jb023280.
22. Wu S, Wang T, Cheng J. Second-order optimization for multiparameter reflection waveform inversion in acoustic VTI media. *Geophys J Int*. 2024;236(1):249-269.  
doi: 10.1093/gji/ggad406
23. Singh S, Tsvankin I, Zabihi Naeini E. Full-waveform inversion with borehole constraints for elastic VTI media. *Geophysics*. 2020;85(6):R553-R563.  
doi: 10.1190/geo2019-0816.1
24. Lang K, Yin X, Zong Z, *et al.* Anisotropic nonlinear inversion based on a novel PP wave reflection coefficient for VTI media. *IEEE Trans Geosci Remote Sens*. 2023;61:1-13.  
doi: 10.1109/TGRS.2023.3295800
25. Wang B, Zhang F, Dai FC, *et al.* Study on seismic inversion method of SH-SH wave in VTI media. *Chin J Geophys*. 2023;66(5):2112-2122. [In Chinese].  
doi: 10.6038/cjg2022P0750
26. Kamath N, Tsvankin I. Elastic full-waveform inversion for VTI media: Methodology and sensitivity analysis. *Geophysics*. 2016;81(2):C53-C68.  
doi: 10.1190/geo2014-0586.1
27. Li V, Tsvankin I, Alkhalifah T. Analysis of RTM extended images for VTI media. *Geophysics*. 2016;81(3):S139-S150.  
doi: 10.1190/geo2015-0384.1
28. Luo C, Ba J, Carcione JM. A hierarchical prestack seismic inversion scheme for VTI media based on the exact reflection coefficient. *IEEE Trans Geosci Remote Sens*. 2022;60:1-16.  
doi: 10.1109/TGRS.2021.3140133
29. Song C, Alkhalifah T, Waheed UB. Solving the frequency-domain acoustic VTI wave equation using physics-informed neural networks. *Geophys J Int*. 2021;225(2):846-859.  
doi: 10.1093/gji/ggab010
30. Ristow D. Migration in transversely isotropic media using implicit finite-difference operators. *J Seism Explor*.



- 1999;8:39-56.
31. Han Q, Wu RS. A one-way dual-domain propagator for scalar qP-waves in VTI media. *Geophysics*. 2005;70(2):D9-D17.  
doi: 10.1190/1.1884826
  32. Bale RA. Phase-Shift Migration and the Anisotropic Acoustic Wave Equation. In: *Proceedings of the 69th EAGE Conference and Exhibition Incorporating SPE EUROPEC 2007*; June 11-14, 2007; London, UK. European Association of Geoscientists & Engineers; 2007:cp-27-00104.  
doi: 10.3997/2214-4609.201401522
  33. Fei TW, Liner CL. Hybrid Fourier finite-difference 3D depth migration for anisotropic media. *Geophysics*. 2008;73(2):S27-S34.  
doi: 10.1190/1.2828704
  34. Bakker PM. A stable one-way wave propagator for VTI media. *Geophysics*. 2009;74(5):WB3-WB17.  
doi: 10.1190/1.3196818
  35. Amazonas D, Aleixo R, Schleicher J, *et al.* Anisotropic complex Padé hybrid finite-difference depth migration. *Geophysics*. 2010;75(2):S51-S59.  
doi: 10.1190/1.3337317
  36. Salcedo M, Novais A, Schleicher J, *et al.* Optimization of the parameters in complex Padé Fourier finite-difference migration. *Geophysics*. 2017;82(3):S259-S269.  
doi: 10.1190/geo2016-0324.1
  37. Liu LN, Zhang JF. Wave equation prestack depth migration method in 3D VTI media. *Chin J Geophys*. 2011;54(6):844-855.  
doi: 10.1002/cjg2.1667
  38. Vyas M, Wang X, Etgen J. One-way TTI propagation: Is it still relevant? In: *SEG Technical Program Expanded Abstracts 2015*; Society of Exploration Geophysicists; 2015:3986-3990.  
doi: 10.1190/segam2015-5915894.1
  39. Alshuhail AA, Verschuur DJ. Robust estimation of vertical symmetry axis models via joint migration inversion: Including multiples in anisotropic parameter estimation. *Geophysics*. 2019;84(1):C57-C74.  
doi: 10.1190/geo2017-0856.1
  40. Wu B, Wu RS, Gao J. Preliminary Investigation of Wavefield Depth Extrapolation by Two-Way Wave Equations. *Int J Geophys*. 2012;2012:968090.  
doi: 10.1155/2012/968090
  41. You J, Wu RS, Liu X, *et al.* Two-way wave equation-based depth migration using one-way propagators on a bilayer sensor seismic acquisition system. *Geophysics*. 2018;83(3):S271-S278.  
doi: 10.1190/geo2017-0172.1
  42. You J, Pan N, Liu W, *et al.* Efficient wavefield separation by reformulation of two-way wave-equation depth-extrapolation scheme. *Geophysics*. 2022;87(4):S209-S222.  
doi: 10.1190/geo2021-0629.1
  43. You JC, Zhang GL, Huang XG, *et al.* Internal-multiple-elimination with application to migration using two-way wave equation depth-extrapolation scheme. *Pet Sci*. 2025;22(1):178-192.  
doi: 10.1016/j.petsci.2024.06.021
  44. Li A, Zhu X, Liu T, *et al.* One-step sparse-matrix method for full wave equation depth migration. *Geophysics*. 2024;89(6):S405-S413.  
doi: 10.1190/geo2023-0372.1
  45. Sandberg K, Beylkin G. Full-wave-equation depth extrapolation for migration. *Geophysics*. 2009;74(6):WCA121-WCA128.  
doi: 10.1190/1.3202535
  46. You J, Cao J. Full-wave-equation depth extrapolation for migration using matrix multiplication. *Geophysics*. 2020;85(6):S395-S403.  
doi: 10.1190/geo2019-0323.1
  47. You J, Sun R, Huang X, Huang J. DeepImaging: Deep neural networks driven full waveform migration. *IEEE Trans Geosci Remote Sens*. 2026;64:5900719.  
doi: 10.1109/TGRS.2025.3648341
  48. Sun R, You J, Li Z, Hu H. Viscoacoustic Full Wavefield Migration and Its Application. *IEEE Trans Geosci Remote Sens*. 2025;63:5914517.  
doi: 10.1109/TGRS.2025.3574991
  49. Alkhalifah T. Traveltime computation with the linearized eikonal equation for anisotropic Media. *Geophys Prospect*. 2002;50(4):373-382.  
doi: 10.1046/j.1365-2478.2002.00322.x
  50. Liu YZ, Wang GY, Dong LG, *et al.* Joint inversion of VTI parameters using nonlinear traveltime tomography. *Chin J Geophys*. 2014;57(10):3402-3410. [In Chinese].  
doi: 10.6038/cjg20141026

## Appendix A

### Appendix A.1. A frequency–wavenumber (FK) filter for removing pseudo-S-waves

To suppress the evanescent waves and pseudo-S-waves in the FK, the vertical wavenumber is reformulated as follows:

$$\begin{cases} k_z^2 = \frac{\omega^2}{v_p^2} \left( \frac{A}{B} \right) \\ A = \omega^2 - v_n^2 (1 + 2\eta) k_x^2 \\ B = \omega^2 - 2v_n^2 \eta k_x^2 \end{cases} \quad (\text{A1})$$

When both parameters  $A > 0$  and  $B > 0$ , the resulting wavefield corresponds to a propagating P-wave. In contrast, if  $A < 0$  and  $B < 0$ , the solution describes a pseudo-S-wave. To suppress these undesired pseudo-S-wave components, the associated one-way propagation operator can be effectively muted by assigning it a value of zero under the condition  $A < 0$  and  $B < 0$ .

To evaluate the effectiveness of removing pseudo-S-waves, a velocity model  $v_p(z, x) = 1500 + 2x + 2z$  was generated, as shown in **Figure A1**, with anisotropic parameters  $\varepsilon = 0.6$  and  $\delta = 0$ . The modeled wavefields with and without removing pseudo-S-waves are shown in **Figure A2**. As indicated with red arrows in **Figure A1**, the pseudo-S-waves can be observed without using the FK filter, while clear P-waves are shown without the pseudo-S-waves when using the FK filter.

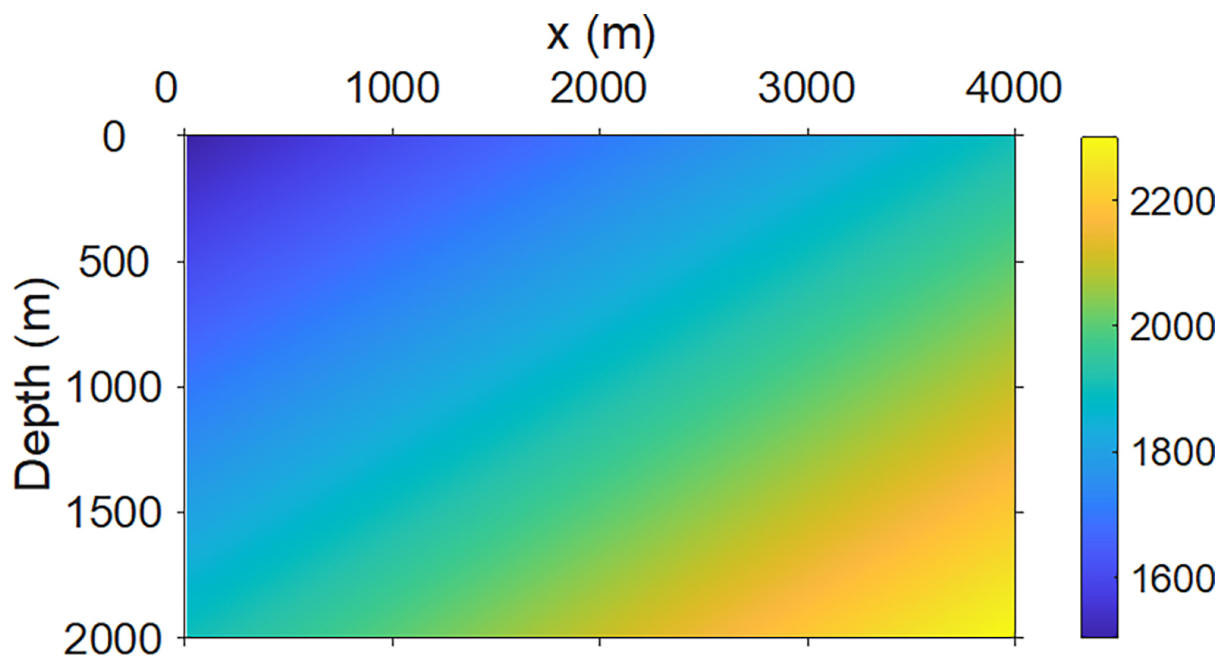


**Figure A1.** Velocity model calculated using  $v_p(z, x) = 1500 + 2x + 2z$

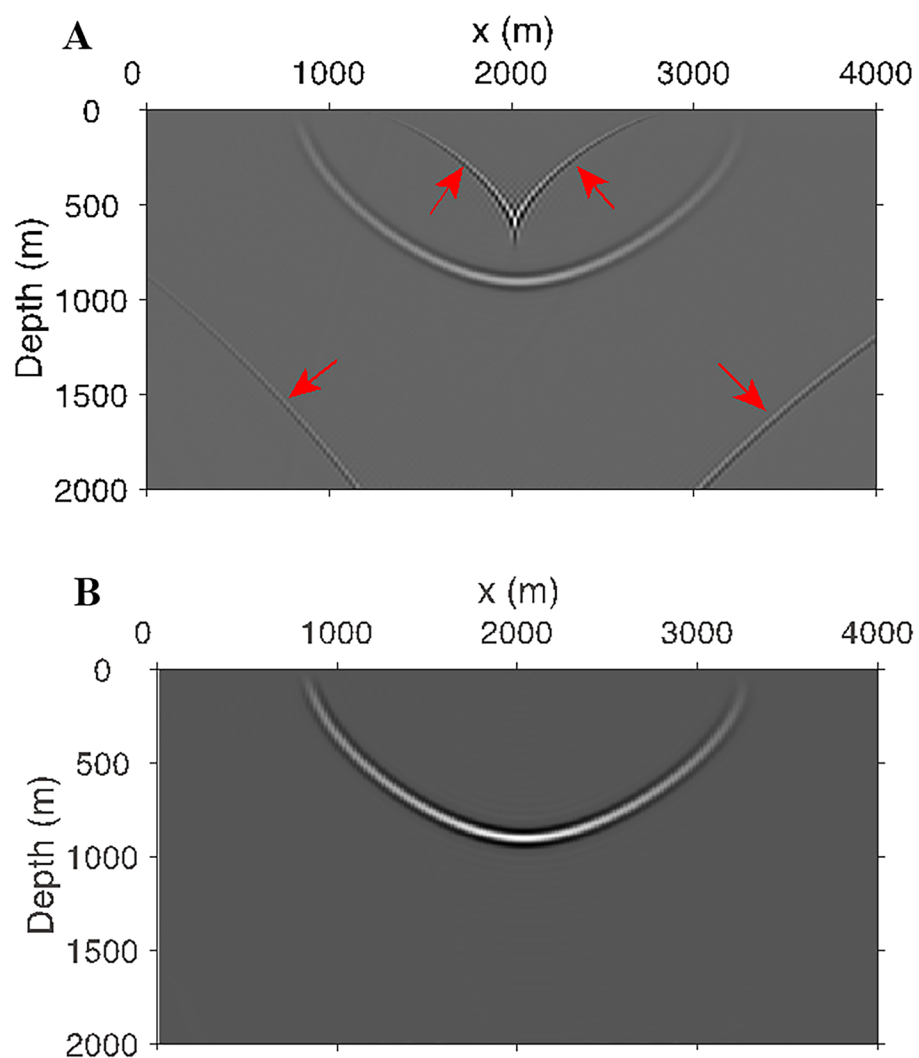


**Figure A2.** Modeled wavefield (A) without removing pseudo-S-waves and (B) with pseudo-S-waves removed. Red arrows indicate pseudo-S-waves.